Reports of NAS RA
ՀՀ ԳԱԱ Զեկույցներ
NATIONAL ACADEMY OF SCIENCES OF THE REPUBLIC OF ARMENIA
ՀԱՅԱՍՏԱՆԻ ՀԱՆՐԱՊԵՏՈՒԹՅԱՆ ԳԻՏՈՒԹՅՈՒՆՆԵՐԻ ԱԶԳԱՅԻՆ ԱԿԱԴԵՄԻԱ

2026 **Volume 126** **Issue 2** **Article No. 3**

Category: Chemistry
Type of Paper: Original Research Article
Received: March 29, 2026, **Revised:** June 17, 2026, **Accepted:** June 22, 2026
Published: June 30, 2026

DOI: 10.54503/0321-1339-2026.126.2-3

Polyiodides of L-ornithine. Discovery of a symmetric (L-Orn(H)-H-L-OrnH) (3+)-cation

Aram M. Petrosyan[1,*], Gerald Giester[2], Milena S. Petrosyan[1], Vahram V. Ghazaryan[1], Ashkhen L. Zatikyan[3]

[1]Institute of Applied Problems of Physics, NAS Armenia, 25 Nersessyan Str., 0014 Yerevan, Armenia
[2]Institute of Mineralogy and Crystallography, University of Vienna, Josef-Holaubek-Platz 2, A-1090 Vienna, Austria
[3]Yerevan State University, 1 Alex Manoogian Str., Yerevan 0025, Armenia

[*]Correspondence: aram.m.petrosyan@gmail.com, apetros@iapp.am

Abstract
Two polyiodides of L-ornithine, (L-OrnH_2)(I_3)(I)(I_2) (I) and (L-Orn(H)-H-L-OrnH)(I_3)$_3$·4H_2O (II) have been synthesized and characterized structurally, by IR, Raman and UV-Vis spectroscopy. Electronic structures of both were determined by quantum chemical calculation based on their structures and bandgaps were measured experimentally as well. Salt (I) is triclinic, space group *P*1 with two formula units in the unit cell, salt (II) crystallizes in the monoclinic space group *C*2 with half of formula unit in the asymmetric unit. A symmetric dimeric cation (L-Orn(H)-H-L-OrnH) was observed in the structure of (II) for the first time.

Keywords: L-Ornithine salts, triiodide, symmetric hydrogen bond, halogen bonding, DFT

1. Introduction

L-Ornithine, L-Orn, (^+H_3N-$(CH_2)_3$-$CH(NH_2)$-COO^-), as well as L-lysine (L-Lys), L-arginine (L-Arg) and L-histidine (L-His), are capable to form salts with both singly charged L-OrnH (^+H_3N-$(CH_2)_3$-$CH(NH_3^+)$-COO^-) and doubly charged L-OrnH_2 (^+H_3N-$(CH_2)_3$-$CH(NH_3^+)$-COOH) cations [1]. On examples of (L-LysH_2···L-LysH)$Cl_2(ClO_4)$ and (L-LysH_2···L-LysH)$Cl_2(NO_3)$ N. Srinivasan et al. [2,3] discovered a new class of salts with a (A^{2+}···A^+) type dimeric cation. These crystals also were the first salts of amino acids containing different anions (see also (GlyH)$_4(Re_2Cl_8)Cl_2$ [4], (L-OrnH_2)$_2$Cl$(NO_3)(SO_4)$ [5] and (BetH)$_2$Cl$(FeCl_4)$ [6]). In [7,8] an analysis of the vibrational spectra of (L-LysH_2···L-LysH)$Cl_2(NO_3)$ and (L-OrnH_2)$_2$Cl$(NO_3)(SO_4)$ was presented. In [9-11] crystals obtained in [2,3] were grown and investigated as possible nonlinear optical materials. We considered this class of salts as a new approach for searching nonlinear optical materials among amino acid salts [12].

More systematic investigations of amino acid salts with different anions and salts with (A^{2+}···A^+) type dimeric cation were carried out in our group [13-23].

In [13] vibrational spectra of (L-LysH_2···L-LysH)$Cl_2(NO_3)$, (L-LysH_2···L-LysH)$Cl_2(BF_4)$ and (L-LysH_2···L-LysH)$Cl_2(ClO_4)$ were investigated and it was shown that the spectra ascribed to (L-LysH_2···L-LysH)$Cl_2(NO_3)$ [7] do not belong to (L-LysH_2···L-LysH)$Cl_2(NO_3)$. Probably they belong to (L-LysH_2)Cl(NO_3) (see [14]). The Raman spectrum of (L-OrnH_2)$_2$Cl$(NO_3)(SO_4)$ [12]

agrees well with that reported in [8] while the IR spectrum differs, presumably due to the use of the KBr pellet method, which can lead to distortions of the spectrum through ion exchange and/or partial decomposition. In addition to salts of L-lysine [14], new mixed salts of other amino acids (L-ornithine, L-histidine, L-arginine and sarcosine) were synthesized and characterized [15-21]. Besides to salts with a dimeric (L-LysH_2···L-LysH) cation, salts with (L-OrnH_2···L-OrnH) [1], (L-HisH_2···L-HisH) [22,1] and (L-ArgH_2···L-ArgH) (see below) cations were also obtained. All these crystals also were mixed salts with different anions. In [23] the first salt was characterized with the (L-HisH_2···L-HisH) cation, but with the same anion, namely (L-HisH_2···L-HisH)$(I)_3$.

Recently, we began a systematic search and investigation of amino acid halogenobismuthates as solar energy converters [24-27]. Among others, we found the salt (L-ArgH_2···L-ArgH)(L-ArgH)$(Bi_4I_{16})\cdot 4H_2O$. It is the first salt with a dimeric cation of the type (L-ArgH_2···L-ArgH) and the second one containing a single type anion. The O···O distance in the short O-H···O hydrogen bridge is 2.497(10) Å.

Various types of halogenobismuthate anions are known [28,29]. The bandgap due to halogenobismuthate anions is about 2 eV [28]. A significant decrease in the bandgap is possible by incorporation of triiodide $(I_3)^-$ anions into the salt's structure [30]. Polyiodides themselves are of great scientific and practical interest [31-37]. To date, a number of amino acid polyiodides have been described [38-43].

In all known (A^{2+}···A^+) type dimeric cations, (L-LysH_2···L-LysH), (L-OrnH_2···L-OrnH), (L-HisH_2···L-HisH) and (L-ArgH_2···L-ArgH), the A^{2+} and A^+ cations are connected by very short, but nonsymmetric hydrogen bonds O-H···O.

In the present paper we report on the synthesis and investigation of two polyiodides of L-ornithine: (L-OrnH_2)$(I_3)(I)(I_2)$ (**I**) and (L-Orn(H)-H-L-OrnH)$(I_3)_3\cdot 4H_2O$ (**II**). Particularly, for the first time an example of the (L-OrnH_2···L-OrnH) cation, but with symmetrical O-H-O hydrogen bond was observed in the structure of (L-Orn(H)-H-L-OrnH)$(I_3)_3\cdot 4H_2O$ (**II**).

2. Experimental and methods

2.1. Materials and synthesis

The starting materials used in experiments were L-ornithine hydrochloride (≥ 99%, FG, Sigma-Aldrich), hydriodic acid (57% w/w, unstabilized, VWR), crystalline iodine (“high purity”, Reakhim) and silver carbonate synthesized from silver nitrate. The components were used according to the following reactions: L-Orn·HCl + $0.5Ag_2CO_3$ + 2HI + $2I_2$ → (L-OrnH_2)$(I_3)(I)(I_2)$ + AgCl↓ + $0.5CO_2$↑ for (**I**), and 2L-Orn·HCl + Ag_2CO_3 + 2.6HI + $2.6I_2$ → (L-Orn(H)-H-L-OrnH)$(I_3)_3\cdot 4H_2O$ + 2AgCl↓ + CO_2↑ for (**II**).

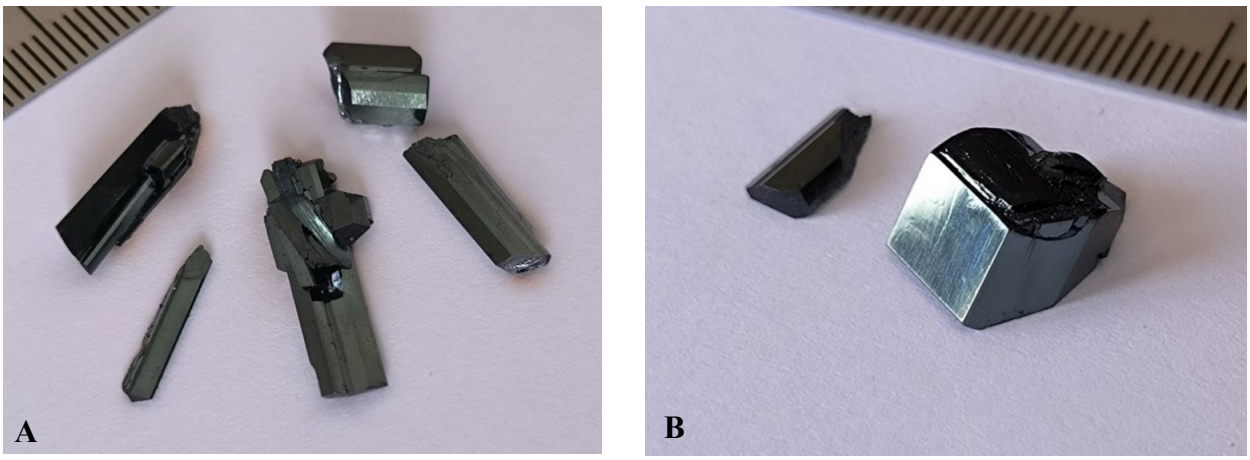

Figure 1. As-grown crystals of **A.** (L-OrnH_2)$(I_3)(I)(I_2)$ (**I**), **B.** (L-Orn(H)-H-L-OrnH)$(I_3)_3\cdot 4H_2O$ (**II**). 1 tick = 1 mm.

For the synthesis of (**II**), the amounts of HI and I_2 were reduced to 2.6 mol relative to the stoichiometric value of 3.0 mol, since pure (**II**) could not be obtained using the stoichiometric ratio. First, Ag_2CO_3 was added to a weighted amount of L-ornithine hydrochloride solution and thoroughly mixed to ensure complete reaction. The AgCl precipitate was removed by filtration through a paper filter. Then HI and I_2 were added to the filtrate and stirred well to achieve a homogenous solution. Crystals of semi-metallic luster, transparent red in thin layers, formed at room temperature by evaporation of the water solvent within a week (Figure 1 A and B).

2.2. Infrared and Raman spectroscopy

Attenuated total reflection Fourier-transform infrared spectra were recorded on an Agilent Cary 630 spectrometer using a germanium ATR sampling module (Ge crystal, Happ-Genzel apodization, ATR distortion corrected, 64 scans, 4 cm^{-1} resolution). The Raman spectra were acquired using a Thermo Scientific DXR3 SmartRaman spectrometer with 785 nm laser source. Data were collected with 2 cm^{-1} resolution, 1 mW laser power, and an aperture slit width of 25 μm.

2.3. Crystal structure determination

Crystal fragments, selected for homogeneous extinction, were mounted on a *MiTeGen* loop with silicone grease. Single crystal X-ray diffraction data at 200K were obtained on a Bruker APEXII diffractometer equipped with a CCD area detector, an Incoatec Microfocus Source IμS (30 W, multilayer mirror, Mo-K_α) and a Cryostream 800 Plus LT device from Oxford Cryosystems. Several sets of omega-scans with a scanwidth of 2° were combined at a crystal-detector distance of 40 mm to obtain corresponding full sphere data up to 65° 2θ. Data collection and processing with integration and absorption correction by evaluating multi-scans was done with the Bruker Apex5 software package [44]. The structures were solved by SHELXT [45] and refined by least-squares techniques using the SHELXL program [46] implemented in the shelXle GUI tool [47].

The crystallographic data as well as details of measurements and refinements are listed in Table 1. Selected bond lengths (Å) and valence angles (°) as well as details of the hydrogen bonding systems are compiled in Tables 2, 3 and 4, 5 for compounds (**I**) and (**II**), respectively. Further details of the crystal structure data may be obtained from the joint CCDC/FIZ Karlsruhe online deposition service: https://www.ccdc.cam.ac.uk/structures/ by quoting the CSD deposition numbers 2540460 (**I**) and 2540459 (**II**).

2.4. Computational method

The present first principle computations were performed using the well-known Cambridge Serial Total Energy Package (CASTEP) [49,50] within the framework of density functional theory (DFT) [51]. Among the various approximations, the generalized gradient approximation (GGA) of the Perdew–Burke–Ernzerhof (PBE) [52] method was chosen as this approximation matched well to gauge the electronic exchange with correlation potentials [53]. The ultrasoft pseudopotential OTFG (On-the-fly generation), based on the DFT theory, was used to describe the electrostatic interaction between ionic core and valence electrons.

2.5. Optical measurements

UV-Vis diffuse reflectance data were acquired on an Agilent Cary 60 UV-Vis spectrophotometer equipped with a Remote Diffuse Reflectance Accessory (DRA). The 100% reflectance baseline was determined using a white PTFE reference plate. Data were registered at room temperature (spectral range 200–1000 nm, scanning rate 10 nm/s, data interval 1.00 nm) on finely powdered crystalline samples.

3. Results and discussion

*3.1. Structure and characterization of (L-OrnH$_2$)(I$_3$)(I)(I$_2$) (**I**)*

*3.1.1. Crystal and molecular structure of (L-OrnH$_2$)(I$_3$)(I)(I$_2$) (**I**)*

Compound (**I**) is triclinic, space group *P*1, with two formula units in the unit cell (Table 1, Fig. 2).

Table 1. Crystallographic data and details of the structure refinement for (L-OrnH$_2$)(I$_3$)(I)(I$_2$) (**I**) and (L-Orn(H)-H-L-OrnH)(I$_3$)$_3$·4H$_2$O (**II**).

Crystal	(**I**)	(**II**)
Empirical Formula	$C_5H_{14}I_6N_2O_2$	$C_{10}H_{35}I_9N_4O_8$
Formula mass	895.58	1481.52
Crystal system	Triclinic	Monoclinic
Space group	*P*1	*C*2
a (Å)	8.2116(6)	24.2160(16)
b (Å)	9.4763(7)	7.7228(5)
c (Å)	12.8884(10)	9.4978(6)
α (°)	73.777(2)	n/a
β (°)	79.217(2)	94.892(2)
γ (°)	73.876(2)	n/a
V (Å^3)	918.56(12)	1769.8(2)
Z, *Z′*	2, 2	2, 0.5
$\rho_{calc.}$(g cm^{-3})	3.238	2.780
Crystal size (mm^3)	0.350×0.200×0.100	0.150×0.125×0.075
Temperature (K)	200(2)	200(2)
$2\theta_{max}$	66.356	66.356
μ (mm^{-1})	10.136	7.916
F(000)	784	1328
Absorption-correction	Multi-scan	Multi-scan
Index ranges	±12, ±14, ±19	±37, ±11, ±14
Reflections collected	34865	39424
Independent reflections (R_{int})	13848/0.0450	6780/0.0283
Data with $F_o > 2\sigma(F_o)$	12654	6239
Parameters refined/restrained	282/5	159/6
Flack parameter [48]	0.02(3)	0.008(12)
R_1/ wR_2 ($I > 2\sigma(I)$) [1]	0.0343/0.0688	0.0219/0.0458
R_1/ wR_2 (for all F_o^2) [1]	0.0388/0.0707	0.0259/0.0476
$\Delta\rho_{fin}$ (max/min) [e Å^{-3}]	1.25/-1.23	1.33/-0.79

[1] $R1 = \Sigma \mid\mid F_o \mid - \mid F_c \mid\mid / \Sigma \mid F_o \mid$; $wR2 = [\Sigma w(F_o^2 - F_c^2)^2 / \Sigma w(F_o^2)^2]^{½}$;
$w = 1 / [\sigma^2(F_o^2) + (a \times P)^2 + b \times P]$; $P = \{[\max \text{ of } (0 \text{ or } F_o^2)] + 2F_c^2\} / 3$

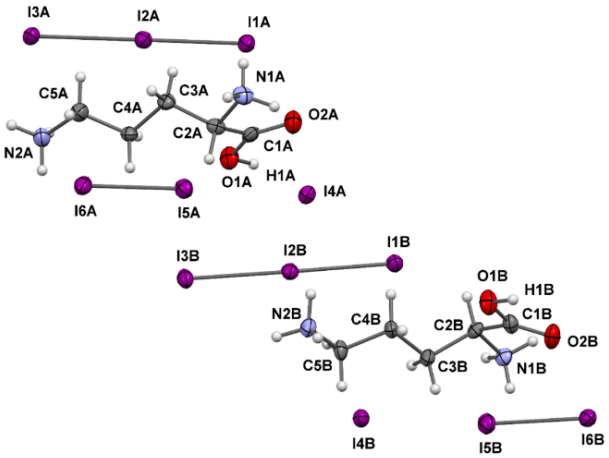

Figure 2. Molecular structure of (L-OrnH$_2$)(I$_3$)(I)(I$_2$) (**I**).

Selected bond lengths and angles are provided in Table 2. Bond lengths, valence- as well as conformational angles of the A- and B- L-ornithinium(2+) cations are comparable. The distances between I1-I2 and I2-I3 differ more significantly in the A-triiodide anion than in the B-anion, with average values of 2.9415 Å and 2.9239 Å, respectively. The bond lengths I5-I6 are similar in the A- and B-molecules. A distinctive feature of structure (**I**) is the presence of both I1-I2-I3 triiodide anions and I4···I5-I6 groups. From the simplified formula (L-OrnH$_2$)(I$_3$)(I)(I$_2$), one might conclude that the structure contains an isolated iodide ion and an iodine molecule. In fact, however, the iodide ion is linked to iodine molecules *via* medium-strength interaction, as in the case of (BetH)(I$_3$) [40]. Intermediate strength bonds typically correspond to I···I lengths in the range of *ca*. 3.0 – 3.5 Å. This interval includes, in particular, the bonds in I_5^- and I_4^- anions. This interval was referred to as "No Man's Land" in [32]. Above 3.5 Å, up to van der Waals interactions (*ca*. 4 Å), supramolecular bonds exist between various polyiodide anions. This emphasizes that they are neither covalent, as in ordinary triiodide-anions, nor supramolecular. In (**I**) actually, ···I6-I5···I4···I6-I5··· groups form chains *via* bonds of the type I4···I5 and I4···I6 with distances of 3.4048 Å, 3.4737 Å and 3.4444 Å, 3.2810 Å for A- and B-moieties, respectively. In contrast to (BetH)(I$_3$) [40], where the corresponding chain has a zigzag geometry, the ···I6-I5···I4···I6-I5··· chain in (**I**) is nearly linear with ∠I6I5I4 (168.29° and 172.11°), ∠I5I4I6 (155.44° and 175.89°) and ∠I4I6I5 (166.51° and 176.06°) angles for A- and B-moieties, respectively. It is also interesting to note that the bond length in one of the iodine molecules in (BetH)(I$_3$) d(I3-I3) = 2.816 Å is very close to the I1-I2 bond length (2.818 Å) in a triiodide anion of (**I**) (Table 2).

Table 2. Selected bond lengths (Å) and angles (°) in the structure of (L-OrnH$_2$)(I$_3$)(I)(I$_2$) (**I**).

Bonds	A	B	Bonds	A	B
C1-O1	1.317(9)	1.317(10)	I1-I2	2.8180(8)	2.9387(7)
C1-O2	1.203(9)	1.185(9)	I2-I3	3.0651(7)	2.9092(7)
C1-C2	1.499(11)	1.529(10)	I5-I6	2.7578(7)	2.7657(7)
C2-N1	1.505(9)	1.506(9)	I1···I3	3.6139(9)	3.8200(8)
C2-C3	1.542(11)	1.533(10)	I4···I5	3.4048(9)	3.4444(9)
C3-C4	1.536(9)	1.524(11)	I4···I6	3.4737(9)	3.2810(9)
C4-C5	1.495(11)	1.502(10)	n/a	n/a	n/a
C5-N2	1.505(10)	1.492(10)	n/a	n/a	n/a
Angles			Angles		
O1-C1-O2	126.4(8)	126.0(8)	I1-I2-I3	177.29(3)	177.06(3)
O1-C1-C2	111.0(6)	110.4(6)	I2-I1···I3	171.59(3)	155.31(2)
O2-C1-C2	122.5(8)	123.6(8)	I2-I3···I1	173.23(2)	158.18(2)
C1-C2-N1	106.0(6)	105.8(6)	I6-I5···I4	168.29(3)	172.11(3)
C1-C2-C3	118.1(6)	117.1(7)	I5-I6···I4	166.51(3)	176.06(3)
N1-C2-C3	108.0(6)	108.9(6)	I5···I4···I6	155.44(2)	175.89(2)
C2-C3-C4	114.8(6)	113.8(6)	n/a	n/a	n/a
C3-C4-C5	108.6(6)	111.6(6)	O2-C1-C2-C3	129.3(9)	125.4(9)
C4-C5-N2	111.8(7)	110.1(6)	C1-C2-C3-C4	73.7(9)	70.6(9)
O1-C1-C2-N1	-174.7(6)	-177.6(6)	N1-C2-C3-C4	-166.0(6)	-169.4(6)
O2-C1-C2-N1	8(1)	4(1)	C2-C3-C4-C5	161.8(7)	163.0(7)
O1-C1-C2-C3	-53(1)	-56.0(9)	C3-C4-C5-N2	171.2(7)	170.1(7)

The packing diagram and arrangement of the anions I1A-I2A-I3A, I1B-I2B-I3B and the groups ···I5A-I6A···I4A···I5A-I6A···, ···I5B-I6B···I4B···I5B-I6B··· in the structure of (**I**) are shown in Fig. 3.

Triiodide anions can exist either free or interconnected *via* supramolecular halogen bonds. In the structure of (L-AlaH···L-Ala)(I$_3$) there are two independent formula units [38] with two triiodide anions formed through the supramolecular bond of the pair I3-I2-I1···I4-I5-I6 with a distance d(I···I)

of 3.8303(9) Å. In the structure of (GlyH)(I_3) [39], triiodide anions form an almost linear chain ···I3-I1-I2···I3-I1-I2··· with a supramolecular bond distance d(I···I) = 3.6145(15) Å.

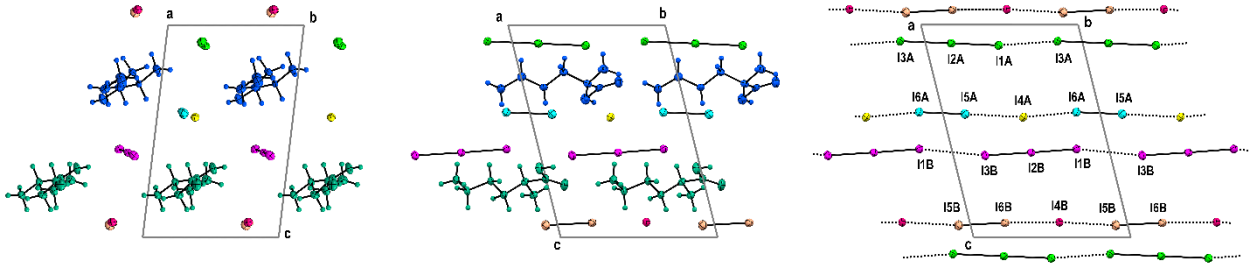

Figure 3. Packing diagram and arrangement of I1A-I2A-I3A, I1B-I2B-I3B anions and ···I5A-I6A···I4A···I5A-I6A···, ···I5B-I6B···I4B···I5B-I6B··· groups in the structure of (L-OrnH_2)(I_3)(I)(I_2) (**I**).

In the structure of [(L-ProH)$_3$(L-Pro)](I_3)$_3$ [40], three triiodide anions are connected by supramolecular halogen bonds as follows: I1-I2-I3···I4-I5-I6···I7- I8-I9 with distances d(I3···I4) and d(I6···I7) of 3.6663(6) Å and 3.6146(6) Å, respectively.

The structures of (L-ProH···L-Pro)(I_3) [41] and (L-ArgH_2)(I_3)$_2$ [42] lack supramolecular halogen bonds. In the structure of L-cystinium(2+) bis-triiodide (L-CsnH_2)(I_3)$_2$, supramolecular bonds form an anionic substructure that differs from those discussed above [43].

In case of (**I**) both triiodide-anions form chains *via* I1···I3 supramolecular bonds with lengths of 3.6139 Å and 3.8200 Å for A- and B-triiodides, respectively.

Parameters of hydrogen bonds in the structure of (**I**) are listed in Table 3. The hydrogen bonds formed by A- and B-cations exhibit both differences and similarities. For example, the carboxyl group of A-cation establishes a hydrogen bond with the I4A ion, while the carboxyl group of the B-cation shows a hydrogen bond with the terminal I3B atom of a triiodide anion. The carbonyl oxygen atom O2A acts as hydrogen bond acceptor of a hydrogen bond with the symmetry-related A-cation, N2A-H21A···O2A^{iv}. A similar hydrogen bond exits for the B-cation, N2B-H21B···O2B^{iv} (Table 3). Both cations also have two C-H···I type contacts, C2A-H2A···I4A^{ii} and C2B-H2B···I1B^{vii}, which may be considered weak hydrogen bonds. All other hydrogen bonds are of an N-H···I type (Table 3).

Table 3. Hydrogen bond parameters (in Å and °) for (L-OrnH_2)(I_3)(I)(I_2) (**I**).

D-H···A	D-H	H···A	D···A	DHA
O1A-H1A···I4A	0.92(4)	2.64(5)	3.543(6)	167(8)
O1B-H1B···I3B ^{i}	0.92(4)	2.75(7)	3.534(6)	143(9)
N1A-H11A···I1A ^{ii}	0.91	2.84	3.643(7)	148
N1A-H11A···I4A ^{ii}	0.91	3.12	3.583(7)	114
N1A-H12A···I4B ^{iii}	0.91	2.72	3.621(7)	171
N2A-H21A···O2A ^{iv}	0.91	2.01	2.860(9)	154
N2A-H22A···I1B ^{iv}	0.91	2.67	3.580(7)	176
N2A-H23A···I3A ^{iv}	0.91	3.00	3.567(7)	122
N2A-H23A···I6A ^{iv}	0.91	3.08	3.843(8)	143
N1B-H11B···I4B ^{v}	0.91	2.83	3.625(6)	147
N1B-H11B···I1B ^{v}	0.91	3.09	3.602(7)	118
N1B-H12B···I3A ^{vi}	0.91	2.69	3.585(7)	169
N1B-H13B···I3B ^{vii}	0.91	2.96	3.805(6)	156
N2B-H21B···O2B ^{iv}	0.91	1.96	2.850(8)	166
N2B-H22B···I4A	0.91	2.78	3.675(7)	169
N2B-H23B···I4B	0.91	2.90	3.673(7)	144
C2A-H2A···I4A ^{ii}	1.00	3.10	3.819(7)	130
C2B-H2B···I1B ^{vii}	1.00	3.04	3.765(8)	130

Symmetry code: (i) x, y+1, z; (ii) x-1, y, z; (iii) x, y, z-1; (iv) x, y-1, z; (v) x+1, y, z; (vi) x, y, z+1; (vii) x+1, y+1, z.

*3.1.2. Infrared and Raman spectra of (L-OrnH$_2$)(I$_3$)(I)(I$_2$) (**I**)*

Fig. 4 shows the infrared and Raman spectra of (L-OrnH$_2$)(I$_3$)(I)(I$_2$). Absorption bands are expected in the high-frequency region caused by stretching modes ν(NH), ν(CH) and possibly ν(OH) of the NH_3^+, CH, CH_2 and COOH groups. In this region a strong broad band with peaks at 3166, 3116, 3082, 3002 and 2904 cm^{-1} is observed. Peaks at 3166, 3116 and 3082 cm^{-1} probably are caused by ν(NH) mode of the NH_3^+ groups, while peaks at 3002 and 2904 cm^{-1} are likely due to the ν(CH) vibration of the CH and CH_2 groups. Due to the lack of reliable correlations of ν(OH) *vs.* R(O···I) distances in the literature, it is difficult to determine where ν(OH) absorption for O-H···I bonds should be expected. The absorption peak at 1719 cm^{-1} is characteristic of the ν(C=O) vibration of carboxyl groups. Other characteristic modes are asymmetric and symmetric deformation vibrations of the NH_3^+ groups at 1596, 1568 and 1541 cm^{-1}; the deformation vibration of CH_2 groups, δ(CH_2) at 1476 and 1459 cm^{-1}; ρ(NH_3^+) at 1183 and 1158 cm^{-1}; the ν(C-N) at 1071, 1052 and 1027 cm^{-1} and ρ(CH_2) at 724 cm^{-1}. The Raman spectrum of (**I**) in the region of triiodide anions and I_2 molecules is also shown in Fig. 4. In the Raman spectrum of crystalline iodine, a line is observed at 180 cm^{-1} [31]. We assign the peak at 158 cm^{-1} to the stretching vibrational mode of the iodine molecules, that at 141 cm^{-1} to the asymmetric stretching mode (ν_3) of the triiodide anion and the one at 65 cm^{-1} to the deformation mode (ν_2). Expected symmetric stretching mode (ν_1) is, probably, obscured as a shoulder near 100-120 cm^{-1} region.

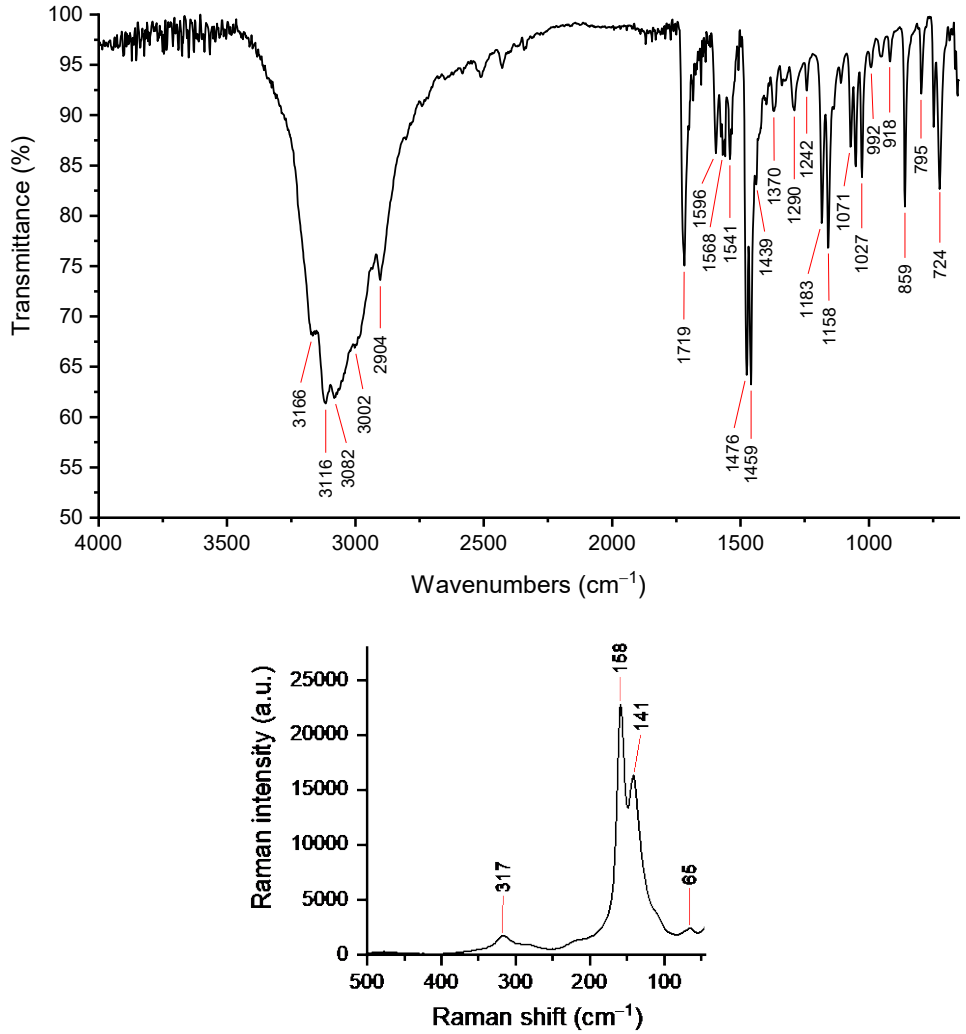

Figure 4. Infrared (top panel) and Raman (bottom panel) spectra of (L-OrnH$_2$)(I$_3$)(I)(I$_2$) (**I**).

3.1.3. DFT calculations and Diffuse reflectance spectra of (L-OrnH$_2$)(I$_3$)(I)(I$_2$) ***(I)***
Band structure (BS) and density of states (DOS)

The electronic band diagram of (I) is presented in Fig. 5 and was calculated employing GGA-PBE potential. The crystallographic data of (I) were used to calculate the electronic band structure and the densities of the states (DOSs) without further optimization. The k-axis was taken for a path along G→F→Q→Z→G of the simulated unit cell.

In the Brillouin region for crystals a k–point mesh of 3 × 3 ×2 was used to calculate the electronic properties.

In a Kohn–Sham computation, the approximation functional used to determine the exchange-correlation energy (Exc) has a significant influence on the accuracy of the results. Relativistic effects were treated using the Koelling-Harmon scalar-relativistic formalism, with an energy range of 10 eV and a k-point separation of 0.005 Å^{-1}. The band energy tolerance lies within 1.0 × 10^{-5} eV per atom.

DFT calculations of (L-OrnH$_2$)(I$_3$)(I)(I$_2$) **(I)**

As evident from the band diagram in Fig. 5, there is no overlap of the valence and conduction bands of crystalline (L-OrnH$_2$)(I$_3$)(I)(I$_2$) **(I)** when using the GGA-PBE potential. The direct transition energy between the highest valence band value and the lowest conduction band value of the Brillion region is 1.153 eV (Fig. 5).

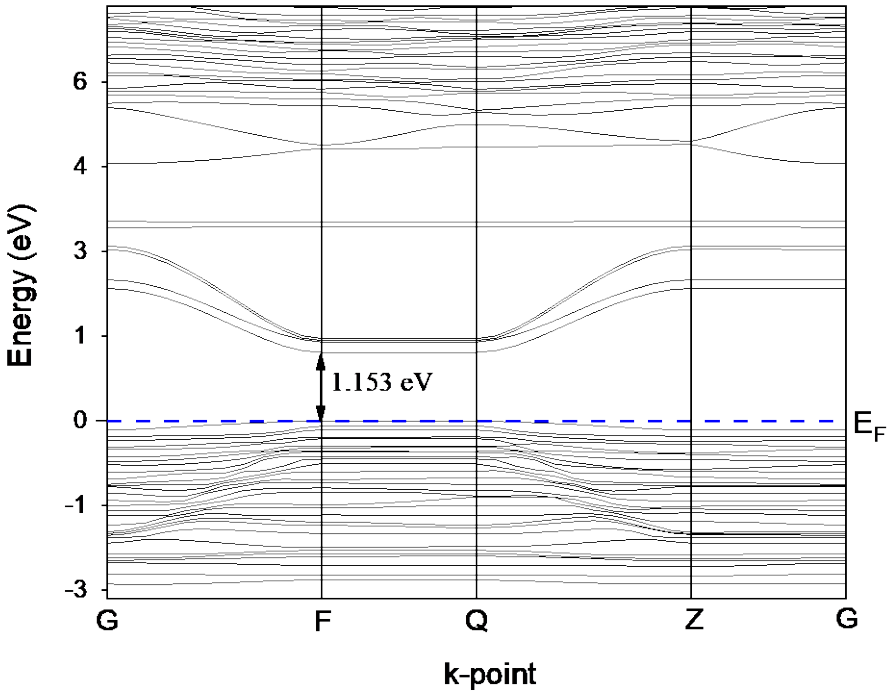

Figure 5. Calculated band structure plot of the (**I**) crystal. The E_F is referred to as the valence band maximum.

Fig. 6 shows the partial and total density of states (PDOS and TDOS) for the valence and conduction bands of the (L-OrnH$_2$)(I$_3$)(I)(I$_2$) **(I)** crystal. The PDOS for the different elements O (2s^2, 2p^4), N (2s^2, 2p^3) and I (5s^2 4d^{10} 5p^5) in the crystal was extracted from the supercell calculations and presented in Fig. 6. It is clearly evident that conduction bands are constructed by the s- and p-orbitals of iodine (I), which hybridize with the N (2p) and O (2p) states.

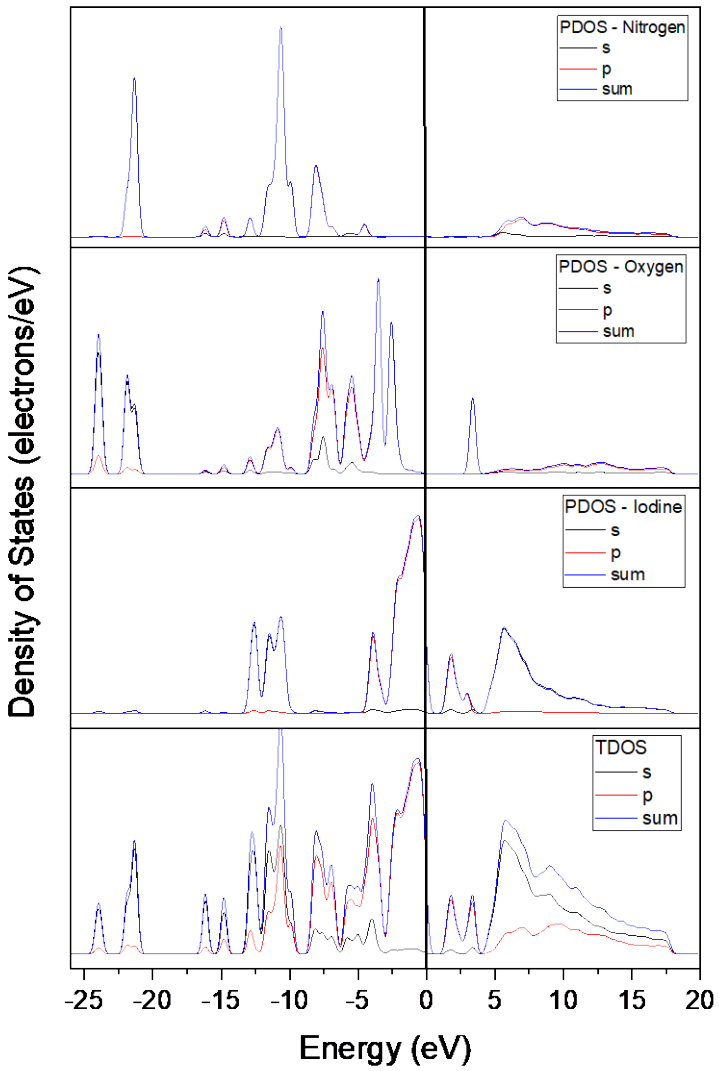

Figure 6. Total (TDOS) and partial (PDOS) density of states for N, O, and I atoms in the (**I**) crystal.

The UV-Vis diffuse reflectance spectrum of (L-OrnH$_2$)(I$_3$)(I)(I$_2$) (Fig. 7) shows an absorption edge in the near-infrared region. The optical bandgap was estimated using the Tauc plots for a direct transition, as determined from DFT calculations, resulting in the value Eg = 1.57 eV.

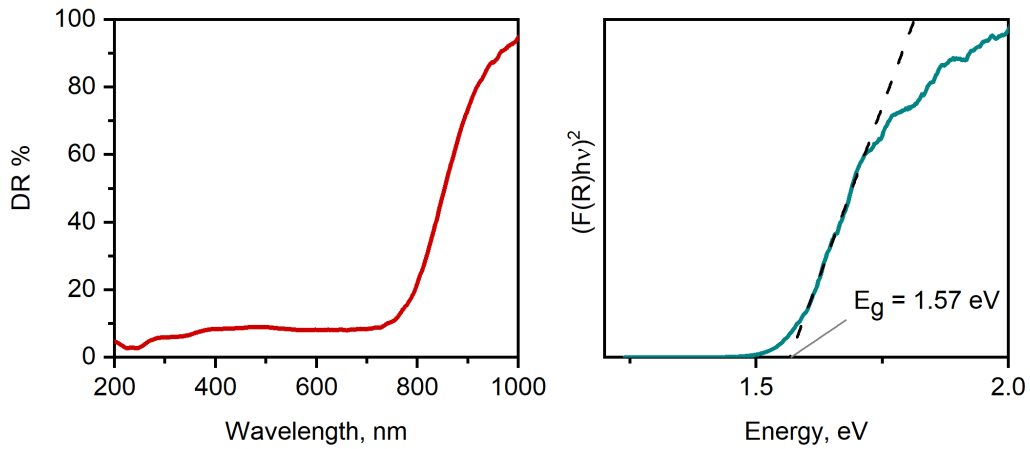

Figure 7. UV-Vis diffuse reflectance spectrum (left) and Tauc plot (right) for direct transition in (L-OrnH$_2$)(I$_3$)(I)(I$_2$).

*3.2. Structure and characterization of (L-Orn(H)-H-L-OrnH)(I3)3·4H2O (**II**)*

*3.2.1. Crystal and molecular structure of (L-Orn(H)-H-L-OrnH)(I3)3·4H2O (**II**)*

The salt (**II**) (Fig. 1B) crystallizes in the monoclinic space group *C*2 (Table 1).

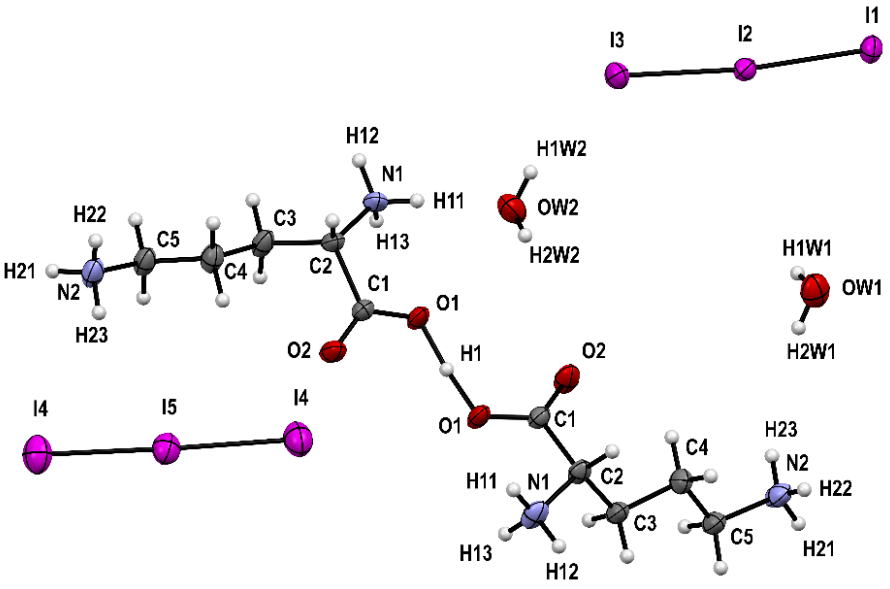

Figure 8. Molecular structure of (L-Orn(H)-H-L-OrnH)$(I_3)_3\cdot 4H_2O$ (**II**).

The molecular structure of (**II**) is shown in Fig. 8. Two H_2O molecules and one triiodide anion (I1-I2-I3) are in general position, while the second anion (I4-I5-I4) and the dimeric cation are centered at special positions (twofold axis). Thus, the dimeric cation of the type ($A^{2+}\cdots A^{+}$) is symmetric in this case, (L-Orn(H)-H-L-OrnH). This is the first observation of a ($A^{+}\cdots H^{+}\cdots A^{+}$) type dimeric cation. Selected bond lengths and angles in the structure of (**II**) are listed in Table 4.

Table 4. Selected bond lengths (Å) and valence angles (°) in the structure of (L-Orn(H)-H-L-OrnH)$(I_3)_3\cdot 4H_2O$ (**II**).

Bonds		Bonds	
C1-O1	1.275(4)	I1-I2	2.9620(3)
C1-O2	1.227(5)	I2-I3	2.8797(4)
C1-C2	1.523(5)	I4-I5	2.9268(4)
C2-N1	1.492(5)	I1···I3	3.8134(4)
C2-C3	1.521(6)	I4···I4	3.7054(5)
C3-C4	1.516(5)	n/a	n/a
C4-C5	1.507(6)	n/a	n/a
C5-N2	1.492(5)	n/a	n/a
Angles		Angles	
O2-C1-O1	126.5(3)	I1-I2-I3	173.38(1)
O2-C1-C2	118.2(3)	I4-I5-I4 [i]	176.83(2)
O1-C1-C2	115.2(3)	I2-I1···I3	156.21(1)
N1-C2-C1	108.4(3)	I2-I3···I1	162.82(2)
N1-C2-C3	110.1(3)	I5-I4···I4	166.86
C1-C2-C3	113.1(3)	O2-C1-C2-C3	-53.7(5)
C2-C3-C4	113.4(4)	O1-C1-C2-C3	126.5(4)
C3-C4-C5	110.3(3)	C1-C2-C3-C4	81.6(5)
C4-C5-N2	111.9(4)	N1-C2-C3-C4	-157.0(4)
O2-C1-C2-N1	-176.1(4)	C2-C3-C4-C5	-177.5(4)
O1-C1-C2-N1	4.1(5)	C3-C4-C5-N2	-177.2(3)

(i) -x+1, y, -z+1

The packing diagram and arrangement of I1-I2-I3 and I4-I5-I4 anions in the structure of (**II**) are shown in Fig. 9 and hydrogen bond parameters are provided in Table 5.

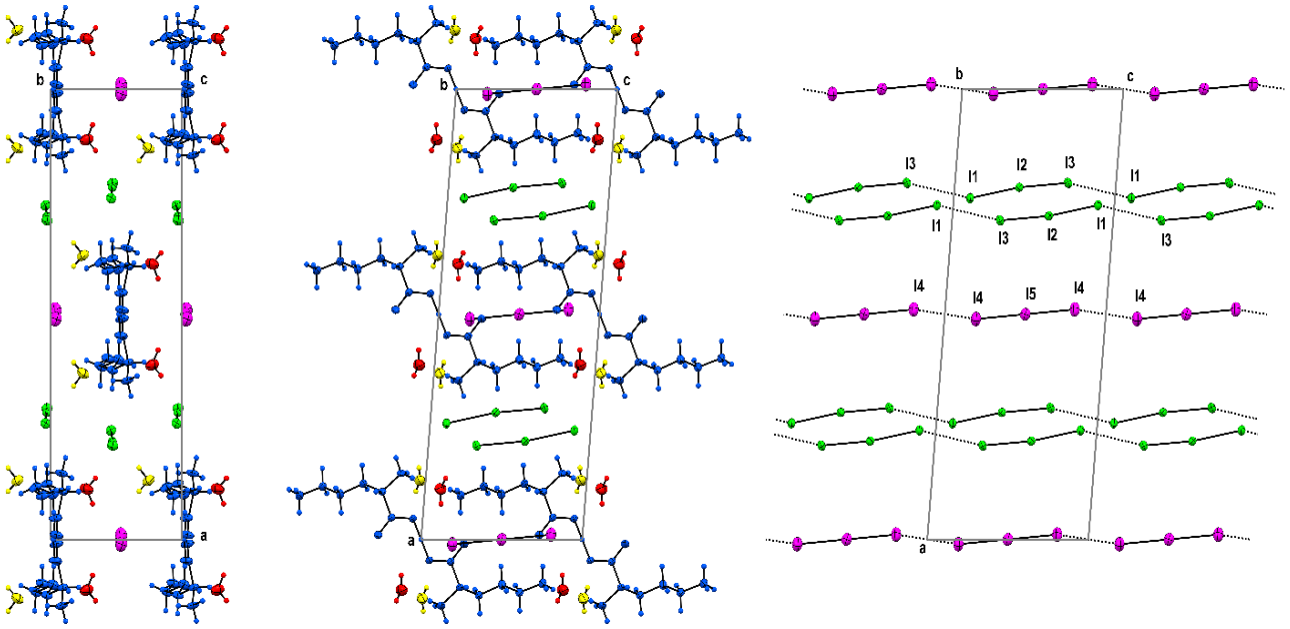

Figure 9. Packing diagram and arrangement of I1-I2-I3 and I4-I5-I4 anions in the structure of (L-Orn(H)-H-L-OrnH)$(I_3)_3 \cdot 4H_2O$ (**II**).

Table 5. Hydrogen bond parameters (in Å and °) for (L-Orn(H)-H-L-OrnH)$(I_3)_3 \cdot 4H_2O$ (**II**).

D-H···A	D-H	H···A	D···A	DHA
O1-H1-O1 [i]	1.222(7)	1.222(7)	2.436(3)	171
N1-H11···OW2 [i]	0.91	1.97	2.866(6)	167
N1-H12···I3 [ii]	0.91	2.97	3.748(4)	144
N1-H13···OW1 [iii]	0.91	1.96	2.857(6)	167
N2-H21···OW1 [iv]	0.91	2.04	2.920(5)	161
N2-H22···OW2 [iii]	0.91	2.03	2.892(7)	158
N2-H23···O2 [iii]	0.91	1.90	2.731(4)	151
OW1-H1W1···I1 [v]	0.89(4)	2.61(4)	3.502(4)	176(4)
OW1-H2W1···I4 [iii]	0.84(4)	2.97(4)	3.758(4)	157(6)
OW2-H1W2···I3	0.83(4)	2.72(4)	3.496(4)	157(7)
OW2-H2W2···I4 [vi]	0.87(4)	2.83(4)	3.667(4)	162(7)

Symmetry code: (i) -x+1, y, -z; (ii) x+1/2, y+1/2, z; (iii) -x+1, y, -z+1; (iv) -x+1, y, -z+2; (v) x, y+1, z; (vi) x, y-1, z.

Of particular interest is the location of carboxyl groups in the structure of (L-Orn(H)-H-L-OrnH)$(I_3)_3 \cdot 4H_2O$, as well as the O···O distance in the symmetric hydrogen bond O-H-O and a comparison of these parameters in structures with dimeric cations of L-ornithine (L-OrnH_2···L-OrnH) and other amino acids with asymmetric hydrogen bonds. A split model (A^+-1/2H^+···1/2H^+-A^+) was also considered, without finding support for it. In this model, the O···O distance is 2.439(3) Å versus 2.436(3) Å, which are close within the error margin and the H1...H1 distance is 0.9(1) Å. In Table 6 some parameters of (A^{2+}···A^+) dimeric cations for (L-Orn(H)-H-L-OrnH)$(I_3)_3 \cdot 4H_2O$ (**II**), (L-OrnH_2···L-OrnH)$(Cl)_2(ClO_4)$ (**III**), (L-OrnH_2···L-OrnH)$(Cl)_2(NO_3)$ (**IV**), (L-LysH_2···L-LysH)$(Cl)_2(ClO_4)$ (**V**), (L-LysH_2···L-LysH)$(Cl)_2(NO_3)$ (**VI**), (L-LysH_2···L-LysH)$(Cl)_2(BF_4)$ (**VII**), (L-LysH_2···L-LysH)$(BF_4)_2(Cl)$ (**VIII**), (L-HisH_2···L-HisH)$(NO_3)(SiF_6)$ (**IX**), (L-HisH_2···L-HisH)$(I)_3$ (**X**), (L-ArgH_2···L-ArgH)(L-ArgH)$(Bi_4I_{16}) \cdot 4H_2O$ (**XI**) are provided.

Table 6. Selected parameters of ($A^{2+}\cdots A^{+}$) dimeric cations for (**II**-**XI**).

#	(O···O)	O-H-O	A^{2+}, C=O	A^{2+}, C-O(H)	A^{+}, C=O	A^{+}, C-O(···H)	Ref.
(**II**)	2.436(3)	171	1.229(5)	1.275(4)	1.229(5)	1.275(4)	*
(**III**)	2.427(4)	144(5)	1.205(6)	1.281(6)	1.218(5)	1.270(4)	[1]
(**IV**)	2.447(10)	137(10)	1.250(9)	1.286(10)	1.221(10)	1.276(9)	[1]
(**V**)	2.453(7)	166	1.203(7)	1.284(8)	1.236(7)	1.250(7)	[2]
(**VI**)	2.425(8)	169(9)	1.217(9)	1.274(9)	1.223(7)	1.267(8)	[3]
(**VII**)	2.431(3)	153	1.213(4)	1.297(4)	1.233(3)	1.269(3)	[13]
(**VIII**)	2.424(4)	148(9)	1.221(4)	1.279(4)	1.219(4)	1.270(4)	[1]
(**IX**)	2.507(2)	159(4)	1.196(3)	1.292(3)	1.247(3)	1.248(3)	[22]
(**X**)	2.498(3)	173(5)	1.236(3)	1.2721(19)	1.242(2)	1.2643(19)	[23]
(**XI**)	2.497(10)	163	1.231(11)	1.306(10)	1.220(11)	1.265(12)	[24]

*this work

Since the symmetric hydrogen bond O-H-O is not centrosymmetric, the carboxyl groups may not lie in the same plane. The torsion angle between the carboxyl groups O1O2O1O2 is 6.4°. The O···O distance is very short, 2.436 Å and is among the smallest listed for the structures in Table 6. It is the average of two values in the structures of (L-OrnH_2···L-OrnH)$(Cl)_2(ClO_4)$ (**III**) and (L-OrnH_2···L-OrnH)$(Cl)_2(NO_3)$ (**IV**). The C-O(H) bond length (1.275 Å) in (**II**) is frequently found in structures with dimeric cations with very short hydrogen bonds. However, the corresponding bond lengths in structures of (**III**) and (**IV**) (1.281 Å and 1.286 Å, respectively) are noticeably higher (Table 6). The values of (**II**) are closest to those of (L-LysH_2···L-LysH)$(Cl)_2(NO_3)$ (**V**) and (L-LysH_2···L-LysH)$(BF_4)_2(Cl)$ (**VIII**).

The bond lengths and angles of asymmetric I1-I2-I3 and symmetric I4-I5-I4 anions are listed in Table 4. Triiodide anions can be symmetric (linear or nearly linear) or asymmetric (nearly linear) [31,32].

The I4-I5 bond length (2.9268(4) Å is not only close to the mean value of I1-I2 and I2-I3 (2.9208 Å), but also to that of the bond lengths of triiodide anions in CSD (2.92 Å) [31]. Both the asymmetric I1-I2-I3 and the symmetric I4-I5-I4 anions are nearly linear with ∠I1-I2-I3 (173.38°) and ∠I4-I5-I4 (176.83°), respectively.

In the structure of (**II**), I1-I2-I3 anions form a nearly linear chain due to the supramolecular halogen bond I1···I3 (3.8134 Å), as do the anions I4-I5-I4 due to the I4···I4 bond (3.7054 Å). The structure of (**II**) is further stabilized *via* hydrogen bonds formed by NH_3^+ groups and H_2O molecules. The N(1)H_3^+ group forms two hydrogen bonds with nearest H_2O molecules and the terminal iodine atom of the adjacent I1-I2-I3 anion, while the N(2)H_3^+ group also is part of two hydrogen bonds with nearest H_2O molecules and the carbonyl oxygen atom of the symmetry-related cation. The H_2O molecules in turn establish hydrogen bonds with both triiodide anions.

*3.2.2. Infrared and Raman spectra of (L-Orn(H)-H-L-OrnH)$(I_3)_3\cdot 4H_2O$ (**II**)*

The infrared and Raman spectra of (L-Orn(H)-H-L-OrnH)$(I_3)_3\cdot 4H_2O$ are shown in Fig. 10. The absorption band near 3400 cm^{-1} is assigned to ν(OH) stretching vibrational modes of H_2O molecules. The peaks at 3167, 3125, 3025 and 2929 cm^{-1} correspond to ν(NH) and ν(CH) stretching modes of NH_3^+, CH and CH_2 groups. The peak at 1749 cm^{-1} is characteristic for ν(C=O) of the carboxyl group. The peaks at 1608, 1568 and 1506 cm^{-1} are probably caused by $\delta_{as}(NH_3^+)$, δ(H_2O) and $\delta_s(NH_3^+)$, that 1466 cm^{-1} by δ(CH_2), the peaks at 1378, 1346 cm^{-1} by ω(CH_2), the one at 1180 cm^{-1} by ρ(NH_3^+), further the peaks at 1101 cm^{-1} by ν(CH) ν(C-N) and 732 cm^{-1} by ρ(CH_2). Fig. 10 shows the Raman spectrum of triiodide anions separately. The peaks at 110 and 146 cm^{-1} are assigned to symmetric and asymmetric stretching modes, respectively.

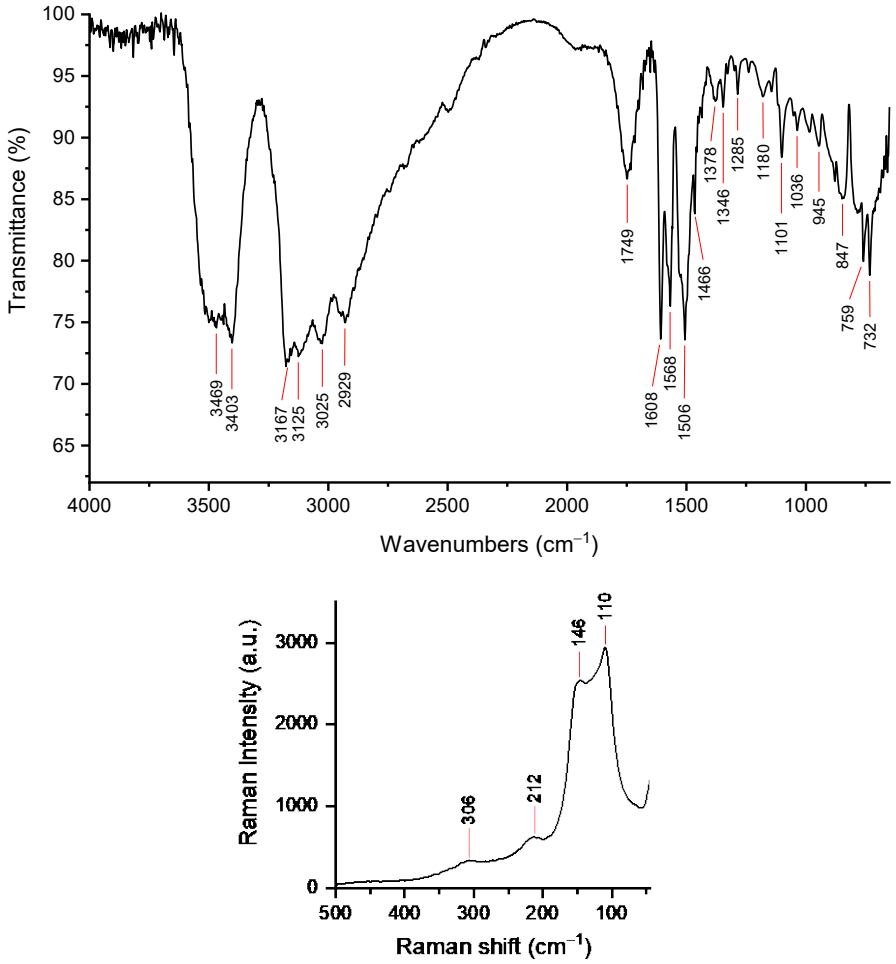

Figure 10. Infrared (top panel) and Raman (bottom panel) spectra of (L-Orn(H)-H-L-OrnH)$(I_3)_3 \cdot 4H_2O$ (**II**).

3.2.3. DFT calculations and Diffuse reflectance spectra of (L-Orn(H)-H-L-OrnH)$(I_3)_3 \cdot 4H_2O$ (II)

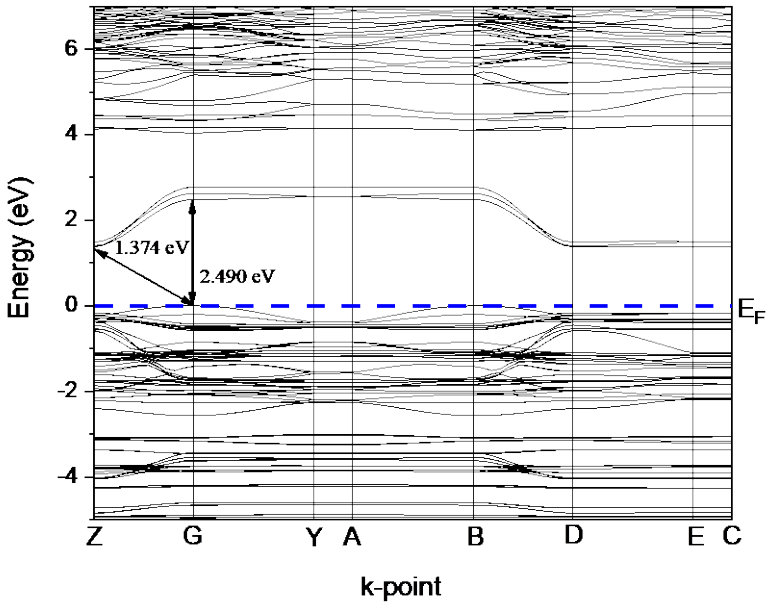

Figure 11. Calculated band structure plot of a (**II**) crystal. The E_F is referred to as the valence band maximum.

As evident from the band diagram in Fig. 11, there is no overlap of the valence and conduction bands of crystalline (**II**) when using the GGA-PBE potential. The direct transition energy between the highest valence band value and the lowest conduction band value of the Brillion region is 2.490 eV, and an indirect bandgap at the Z→G range is 1.374 eV (Fig. 11).

The presence of the groups ⋯I5A-I6A⋯I4A⋯I5A-I6A⋯, ⋯I5B-I6B⋯I4B⋯I5B-I6B⋯ in the form of one long chain in the structure of (L-OrnH$_2$)(I$_3$)(I)(I$_2$) (**I**), in which the electron is delocalized over the entire chain length, leads to a direct transition energy, in contrast to the compound (L-Orn(H)-H- L-OrnH)(I$_3$)$_3$·4H$_2$O (**II**).

Fig. 12 shows the partial and total density of states (PDOS and TDOS) for the valence and conduction bands of the crystal (L-Orn(H)-H- L-OrnH)(I$_3$)$_3$·4H$_2$O **(II)**. From the supercell calculations, the PDOS for the different elements O ($2s^2$, $2p^4$), N ($2s^2$, $2p^3$) and I ($5s^2$ $4d^{10}$ $5p^5$) in the crystal was extracted and presented in Fig. 12. It is again evident that conduction bands are formed by the s- and p-orbitals of iodine (I), which hybridize with the N (2p) and O (2p) states.

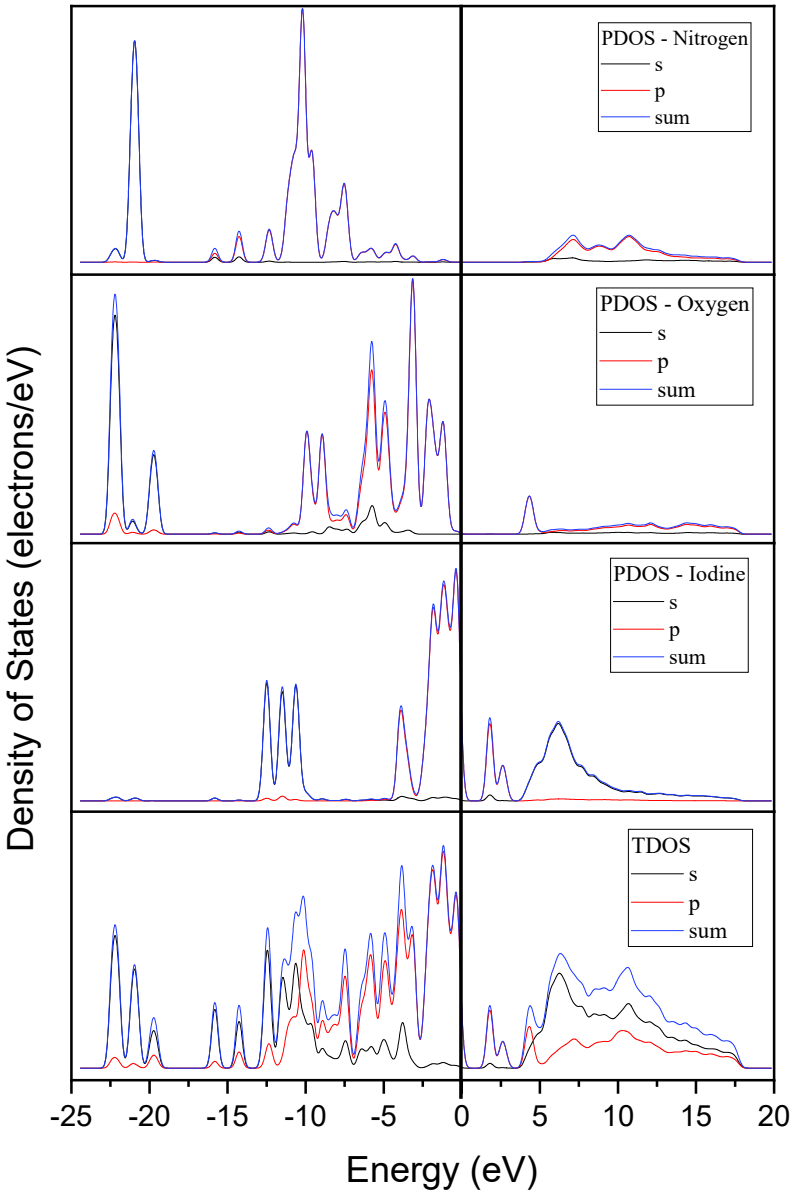

Figure 12. Total (TDOS) and partial density (PDOS) of states for N, O, and I atoms in the crystal (**II**).

The UV-Vis diffuse reflectance spectrum of (L-Orn(H)-H-L-OrnH)$(I_3)_3 \cdot 4H_2O$ (Fig. 13) shows an absorption edge similar to (**I**). The optical bandgap for an indirect transition, as derived from DFT calculations, is Eg = 1.47 eV.

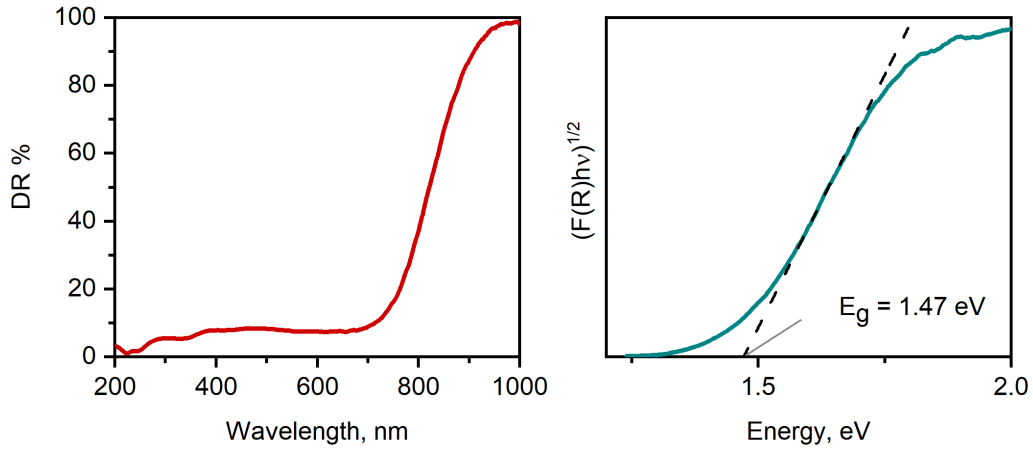

Figure 13. UV-Vis diffuse reflectance spectrum (left) and Tauc plot (right) for indirect transitions in (**II**).

4. Conclusions

Two new polyiodide salts of L-ornithine were synthesized and comprehensively characterized. Compound (L-$OrnH_2$)$(I_3)(I)(I_2)$ (**I**) exhibits a complex polyiodide network composed of triiodide anions and I···I interactions of intermediate strength, forming nearly linear chains. Compound (L-Orn(H)-H-L-OrnH)$(I_3)_3 \cdot 4H_2O$ (**II**) contains three triiodide anions and H_2O molecules stabilizing the structure *via* hydrogen bonding.

The most important discovery is the formation of a symmetric (L-Orn(H)···H··· L-OrnH)$^{3+}$ dimeric cation featuring a centered proton within a short O-H-O hydrogen bond (O···O = 2.436(3) Å). This represents the first confirmed example of a symmetric dimeric cation of the type ($A^+ \cdots H^+ \cdots A^+$) in amino acid salts, in contrast to previously reported asymmetric ones. DFT calculations reveal iodine-dominated electronic states near the band edges.

References

[1] M. Fleck, A.M. Petrosyan, Salts of amino acids: crystallization, structure and properties. Springer, Dordrecht, 2014. https://doi.org/10.1007/978-3-319-06299-0

[2] N. Srinivasan, B. Sridhar, R.K. Rajaram, Hydrogen bis[L-lysinium(2+) dichloride perchlorate. Acta Crystallogr. E57, o875-o877 (2001). https://doi.org/10.1107/S1600536801013484

[3] N. Srinivasan, B. Sridhar, R.K. Rajaram, L-lysine L-lysinium dichloride nitrate. Acta Crystallogr. E57, o888-o890 (2001). https://doi.org/10.1107/S1600536801014040

[4] A.V. Shtemenko, O.V. Kozhura, A.A. Pasenko, K.V. Domasevitch, New octachlorodirhenate(III) salts: solid state manifestation for a certain conformational flexibility of the $[Re_2Cl_8]^{2-}$ ion. Polyhedron 22 (2003) 1547-1552. https://doi.org/10.1016/S0277-5387(03)00288-2

[5] S. Ramaswamy, B. Sridhar, V. Ramakrishnan, R.K. Rajaram, Bis(L-ornithinium) chloride nitrate sulfate. Acta Crystallogr. E60 (2004) o768-o770. https://doi.org/10.1107/S1600536804007238

[6] T. Bäcker, A.-V. Mudring, Betaine chloride-betaine tetrachloridoferrate(III)- an ionic liquid related crystal structure governed by the Pearson concept. Crystals 2 (2012) 110-117. https://doi.org/10.3390/cryst2010110

[7] M. Briget Mary, M. Umadevi, V. Ramakrishnan, Vibrational spectral analysis of L-lysine L-lysinium dichloride nitrate. Spectrochim. Acta A Mol Biomol Spectrosc. 61 (2005) 3124-3130. https://doi.org/10.1016/j.saa.2004.11.045
[8] S. Ramaswamy, R.K. Rajaram, V. Ramakrishnan, Vibrational spectra of bis(*L*-ornithinium) chloride nitrate sulfate. J. Raman Spectr. 36(1) (2005) 12-17. https://doi.org/10.1002/jrs.1257
[9] V. Vasudevan, R. Ramesh Babu, A. Reicher Nelcy, Bhagavannarayana, K. Ramamurthi, Synthesis, growth, optical, mechanical and electrical properties of *L*-lysine *L*-lysinium dichloride nitrate (*L*-LLDN) single crystal. Bull. Mater. Sci. 34 (2011) 469-475. https://doi.org/10.1007/s12034-011-0123-3
[10] V. Vasudevan, R. Ramesh Babu, K. Ramamurthi, Unidirectional growth of L-lysine L-lysinium dichloride nitrate (L-LLDN) single crystals by the SR method. Physica B 406 (2011) 936-940. https://doi.org/10.1016/j.physb.2010.12.031
[11] V. Vasudevan, R. Ramesh Babu, K. Ramamurthi, Synthesis, growth and characterization of L-lysinium…L-lysinium(2+) dichloride perchlorate (LLDP) single crystals by Sankaranarayanan-Ramasamy method. Spectrochim. Acta A99 (2012) 259-265. https://doi.org/10.1016/j.saa.2012.09.027
[12] A.M. Petrosyan, H.A. Karapetyan, V.V. Ghazaryan, New approach for searching nonlinear optical materials among salts of amino acids. Proc. conf. "Laser Physics-2008" 14-17 Oct. 2008, Ashtarak, Armenia, pp. 63-66 (2009).
[13] V.V. Ghazaryan, M. Fleck, A.M. Petrosyan, Mixed salts of amino acids: On the vibrational spectra of mixed salts containing a *L*-lysinium(+)...*L*-lysinium(2+) dimeric cation. J. Mol. Struct. 982 (2010) 145-151. https://doi.org/10.1016/j.molstruc.2010.08.020
[14] V.V. Ghazaryan, M. Fleck, A.M. Petrosyan, Mixed salts of amino acids: *L*-lysinium(2+) chloride nitrate, *L*-lysinium(2+) chloride tetrafluoroborate and *L*-lysinium(2+) chloride perchlorate. J. Mol. Struct. 984 (2010) 268-275. https://doi.org/10.1016/j.molstruc.2010.09.039
[15] A.M. Petrosyan, M. Fleck, V.V. Ghazaryan, Mixed salts of amino acids: Syntheses, crystal structure and vibrational spectra of *L*-histidinium(2+) nitrate-perchlorate and *L*-histidinium(2+) nitrate-tetrafluoroborate. Z. Kristallogr. 225 (2010) 388-395. https://doi.org/10.1524/zkri.2010.1269
[16] V.V. Ghazaryan, M. Fleck, A.M. Petrosyan, Mixed salts of amino acids: new analogs of the di-*L*-ornithinium(2+) chloride nitrate sulfate crystal. J. Cryst. Phys. Chem. 2 (2011) 7-16.
[17] V.V. Ghazaryan, M. Fleck, A.M. Petrosyan, Salts of amino acids with hexafluorosilicate anion. J. Cryst. Growth 362 (2013) 162-166. https://doi.org/10.1016/j.jcrysgro.2011.11.017
[18] V.V. Ghazaryan, M. Fleck, A.M. Petrosyan, Mixed salts of amino acids with different anions. J. Cryst. Growth 362 (2013) 182-188. https://doi.org/10.1016/j.jcrysgro.2011.09.059
[19] M. Fleck, V.V. Ghazaryan, A.M. Petrosyan, Mixed salts of amino acids: *L*-ornithinium(2+) sulfate hydrogen fluoride and tri-*L*-ornithinium(2+) dinitrate disulfate. JUET Res. J. Sci. Technol. 1(1) (2014) 11-25.
[20] A.M. Petrosyan, M. Fleck, V.V. Ghazaryan, New mixed salts of *L*-histidinium(2+) comprising hexafluorosilicate anion. J. Cryst. Growth 401 (2014) 863-868. https://doi.org/10.1016/j.jcrysgro.2013.10.060
[21] G. Giester, V.V. Ghazaryan, M. Fleck, S. Thamotharan, M.J. Percino, A.M. Petrosyan, Mixed salt of sarcosine containing dimeric undecafluoridodialuminate anion and fluoride ion. J. Fluor. Chem. 209 (2018) 73-78. https://doi.org/10.1016/j.jfluchem.2018.02.011
[22] V.V. Ghazaryan, M. Fleck, A.M. Petrosyan, Mixed salts of amino acids: *L*-histidinium(+)...*L*-histidinium(2+) nitrate-hexafluorosilicate. J. Mol. Struct. 1026 (2012) 140-144. https://doi.org/10.1016/j.molstruc.2012.05.052
[23] G. Giester, V.V. Ghazaryan, M. Fleck, G.S. Tonoyan, A.M. Petrosyan, L-histidine iodides. J. Mol.

Struct. 1182 (2019) 317-326. https://doi.org/10.1016/j.molstruc.2019.01.068
[24] Aram Petrosyan, Gerald Giester, Vahram Ghazaryan, Gayane Tonoyan, Marek Szafrański, Artak Mkrtchyan, Halogenobismuthates of amino acids as solar energy converters. Armenian Patent # 751 Y. Official Gazette 2/07/2022, p.8.
[25] V.V. Ghazaryan, G. Giester, A.L. Zatikyan, G.S. Tonoyan, A.M. Petrosyan, Hexahalogenobismuthates of Glycine. J. Phys. Conf. Ser. 2924 (2024) 012012. https://doi.org/10.1088/1742-6596/2924/1/012012
[26] A.M. Petrosyan, G. Giester, A.L. Zatikyan, V.V. Ghazaryan, Bromo- and iodobismuthates of L-proline with a ($A^+\cdots A^+$) type dimeric and a new type of tetrameric cations. Struct. Chem. 37 (2026) 687-700. https://doi.org/10.1007/s11224-025-02570-y
[27] A.M. Petrosyan, G. Giester, V.V. Ghazaryan, G.S. Tonoyan, G.A. Tonoyan, M. Szafrański, Synthesis, crystal growth and characterization of iodo- and bromobismuthates of sarcosine with sarcosinium···sarcosinium dimeric cation. ACS OMEGA 2026 11 (2026), 29099-29108. https://doi.org/10.1021/acsomega.6c02514
[28] L.-M. Wu, X.-T. Wu, L. Chen, Structural overview and structure–property relationships of iodoplumbate and iodobismuthate. Coord. Chem. Rev. 253 (2009) 2787–2804. https://doi.org/10.1016/j.ccr.2009.08.003
[29] S.A. Adonin, M.N. Sokolov, V.P. Fedin, Polynuclear halide complexes of Bi(III): From structural diversity to the new properties. Coord. Chem. Rev. 312 (2016) 1-21. https://doi.org/10.1016/j.ccr.2015.10.010
[30] W. Zhang, X. Liu, L. Li, Zh. Sun, Sh. Han, Zh. Wu, J. Luo, Triiodide-induced band-edge reconstruction of a lead-free perovskite-derivative hybrid for strong light absorption. Chem. Mater. 30 (2018) 4081-4088. https://doi.org/10.1021/acs.chemmater.8b01200
[31] P.H. Svensson, L. Kloo, Synthesis, structure, and bonding in polyiodide and metal iodide-iodine systems. Chem. Rev. 103 (2003) 1649-1684. https://doi.org/10.1021/cr0204101
[32] M. Savastano, Words in supramolecular chemistry: the ineffable advances of polyiodide chemistry. Dalton Trans. 50 (2021) 1142-1165. https://doi.org/10.1039/D0DT04091F
[33] M. Savastano, H.H. Osman, Á. Vegas, F.J. Manjón, Rethinking polyiodides: the role of electron-deficient multicenter bonds. Chem. Commun. 60 (2024), 12677-12689. https://doi.org/10.1039/D4CC02832E
[34] H.H. Osman, P. Rodríguez-Hernándes, A. Muñoz, F.J. Manjón, A unified theory of electron-rich and electron-deficient multicenter bonds in molecules and solids: a change of paradigms. J. Mater. Chem. C 13 (2025) 3774- 3803. https://doi.org/10.1039/D4TC04441J
[35] E. Bandiello, Á. Lobato, F. Izquierdo, H.H. Osman, A. Muñoz, P. Rodríguez-Hernándes, F.J. Manjón, From polyanions to infinite chains: chemical bonding evalution in AX_3 polyhalides under pressure. J. Mater. Chem. C 13 (2025) 21936-21946. https://doi.org/10.1039/D5TC01566A
[36] M. Sulli, A. Bianchi, C. Bazzicalupi, M. Savastano, Incommensurately modulated sodium polyiodide crystal structure discloses unconventional 1D iodide chains. Cell Rep. Phys. Sci. 6 (2025), 102925. https://doi.org/10.1016/j.xcrp.2025.102925
[37] M. Savastano, The acid-base concept in modern supramolecular chemistry. Coord. Chem. Rev. 549 (2026) 217308. https://doi.org/10.1016/j.ccr.2025.217308
[38] M. Fleck, Ch. Lengauer, L. Bohatý, E. Tillmanns, Synthesis, crystal structures and thermal behaviour of novel L-alanine halogenide compounds. Acta Chim. Slov. 55 (2008) 880-888.
[39] T.A. Shestimerova, M.A. Bykov, Z. Wei, E.V. Dikarev, A.V. Shevelkov, Crystal structure and two-level supramolecular organization of glycinium triiodide. Russ. Chem. Bull., Intern. Edition 68 (2019) 1520-1524. https://doi.org/10.1007/s11172-019-2586-0

[40] G. Giester, A.L. Zatikyan, G.S. Tonoyan, V.V. Ghazaryan, M. Szafrański, A.M. Petrosyan, Polyiodides of amino acids. Betainium triiodide. J. Mol. Struct. 1297(1) (2024) 136960. https://doi.org/10.1016/j.molstruc.2023.136960
[41] G. Giester, V.V. Ghazaryan, A.L. Zatikyan, A.M. Petrosyan, Polyiodides of amino acids. L-Proline triiodides. Struct. Chem. 35(5) (2024), 1399-1409. https://doi.org/10.1007/s11224-024-02291-8
[42] A.M. Petrosyan, G. Giester, G.S. Tonoyan, V.V. Ghazaryan, A.L. Zatikyan, R.Yu. Chilingaryan, A.A. Margaryan, A.H. Mkrtchyan, Iodides and polyiodides of L-arginine. J. Mol. Struct. 1321 (2025) 139688. https://doi.org/10.1016/j.molstruc.2024.139688
[43] A.M. Petrosyan, G. Giester, M.S. Petrosyan, V.V. Ghazaryan, A.L. Zatikyan, Preparation and characterization of L-cystinium(2+) bis-iodide monohydrate and L-cystinium(2+) bis-triiodide. Struct. Chem. 36 (2025) 2131-2142. https://doi.org/10.1007/s11224-025-02495-6
[44] Bruker (2023) APEX5 software suite. Bruker AXS Inc., Madison, Wisconsin, USA.
[45] G.M. Sheldrick, SHELXT – Integrated space-group and crystal-structure determination. Acta Crystallogr. A71 (2015) 3-8. https://doi.org/10.1107/S2053273314026370
[46] G.M. Sheldrick, Crystal structure refinement with SHELXL. Acta Crystallogr. C71 (2015), 3-8. https://doi.org/10.1107/S2053229614024218
[47] C.B. Hübschle, G.M. Sheldrick, B. Dittrich, ShelXle: a Qt graphical user interface for SHELXL. J. Appl. Cryst. 44 (2011) 1281-1284. https://doi.org/10.1107/S0021889811043202
[48] S. Parsons, H.D. Flack, T. Wagner, Use of intensity quotients and differences in absolute structure refinement. Acta Crystallogr. B69 (2013) 249-259. https://doi.org/10.1107/S2052519213010014
[49] S.J. Clark, M.D. Segall, C.J. Pickard, P.J. Hasnip, M.I.J. Probert, K. Refson, M.C. Payne, First principles methods using CASTEP. Z. Kristallogr. 220 (2005) 567-570. https://doi.org/10.1524/zkri.220.5.567.65075
[50] M.D. Segall, P.J.D. Lindan, M.J. Probert, C.J. Pickard, P.J. Hasnip, S.J. Clark, M.C. Payne, First-principles simulation: ideas, illustrations and the CASTEP code. J. Phys.: Condens. Matter 14 (2002) 2717-2744. https://doi.org/10.1088/0953-8984/14/11/301
[51] P. Hohenberg, W. Kohn, Inhomogeneous electron gas. Phys. Rev. 136 (1964) B864. https://doi.org/10.1103/PhysRev.136.B864
[52] J.P. Perdew, A. Ruzsinszky, G.I. Csonka, O.A. Vydrov, G.E. Scuseria, L.A. Constantin, X. Zhou, K. Burke, Restoring the density-gradient expansion for exchange in solids and surfaces. Phys. Rev. Lett. 100 (2008) 136406. https://doi.org/10.1103/PhysRevLett.100.136406
[53] H.-H. Li, Q.-S. Zheng, Z.-R. Chen, H.-J. Dong, Y.-L. Wu, M. Wang, Reduced band gap in $[Pb_2I_4(datone)_2]_n$: synthesis, properties and calculations. J. Mol. Struct. 982 (2010) 28-32. https://doi.org/10.1016/j.molstruc.2010.07.037

Author's Contributions: AP: Conceptualization, methodology, writing—original draft; GG: Investigation, formal analysis, writing-review, editing; MP: Investigation, writing; VGh: Investigation, writing—review, editing, visualization; AZ: Investigation, writing—review, editing, visualization.
Funding: The research was supported by the Higher Education and Science Committee of MESCS RA (Research project No. 21AG-1D015). A.Z. also expresses gratitude to the Higher Education and Science Committee of MESCS RA (YSU-CHEM research project) for support.
Conflicts of Interest: The authors declare no conflicts of interest.